Water nanodroplet thermodynamics : quasi-solid phase boundary dispersivity

Zhang, Xi; Sun, Peng; Huang, Yongli; Ma, Zengsheng; Liu, Xinjuan; Zhou, Ji; Zheng, Weitao; Sun, Chang Qing

2015

Zhang, X., Sun, P., Huang, Y., Ma, Z., Liu, X., Zhou, J., et al. (2015). Water nanodroplet thermodynamics : quasi-solid phase-boundary dispersivity. The Journal of Physical Chemistry B, 119(16), 5265-5269.

https://hdl.handle.net/10356/96193

https://doi.org/10.1021/acs.jpcb.5b00773

Water nanodroplet thermodynamics: quasi-solid phase-boundary dispersivity

Peng Sun[1], Xi Zhang,[2] Yongli Huang,[3] Zengsheng Ma,[3] Xinjuan Liu,[1] Ji Zhou,[4] Weitao Zheng,[5] and Chang Q Sun[6]

1. *Institute for Coordination Bond Metrology and Engineering, College of Materials Science and Engineering, China Jiliang University, Hangzhou 310018, China*
2. *Institute of Nanosurface Science and Engineering, Shenzhen University, Shenzhen 518060, China*
3. *Key Laboratory of Low-dimensional Materials and Application Technology (MOE) and School of Materials Science and Engineering, Xiangtan University, Xiangtan, 411105, China*
4. *State Key Laboratory of New Ceramics and Fine Processing, Department of Materials Science and Engineering, Tsinghua University, Beijing 100084, China*
5. *School of Materials Science, Jilin University, Changchun 130012, China*
6. *NOVITAS, School of Electrical and Electronic Engineering, Nanyang Technological University, Singapore 639798*

Abstract

It has long been puzzling that water nanodroplet undergoes simultaneously "supercooling" at freezing and "superheating" at melting. Recent progress [Sun et al., *J Phys Chem Lett* 2013, **4**: 2565; *ibid*, **4**: 3238] enables us to resolve this anomaly from the perspective of hydrogen bond (O:H-O) specific-heat disparity. A superposition of the specific-heat η_x(T) curves for the H-O bond (x = H) and the O:H nonbond (x = L) defines two intersecting temperatures that form boundaries of the quasi-solid phase between ice and liquid water. Molecular undercoordination (with fewer than four nearest neighbours in the bulk) stretches the η_H(T) curve by raising the Debye temperature Θ_{DH} through H-O bond shortening and phonon stiffening. The η_H(T) stretching is coupled with the η_L(T) depressing because of the Coulomb repulsion between electron pairs on oxygen ions. The extent of dispersion varies with the size of a droplet that prefers a core-shell structure configuration – the bulk interior and the skin. Understandings may open an effective way of dealing with the thermodynamic behaviour of water droplets and bubbles from the perspective of O:H-O bond cooperativity.

Keywords: Nanodroplet; supercooling; superheating; specific heat; hydrogen bond

Content entry

Molecular undercoordination raises its melting point and lowers its freezing by dispersing boundaries of quasi-solid phase through O:H-O bond relaxation.

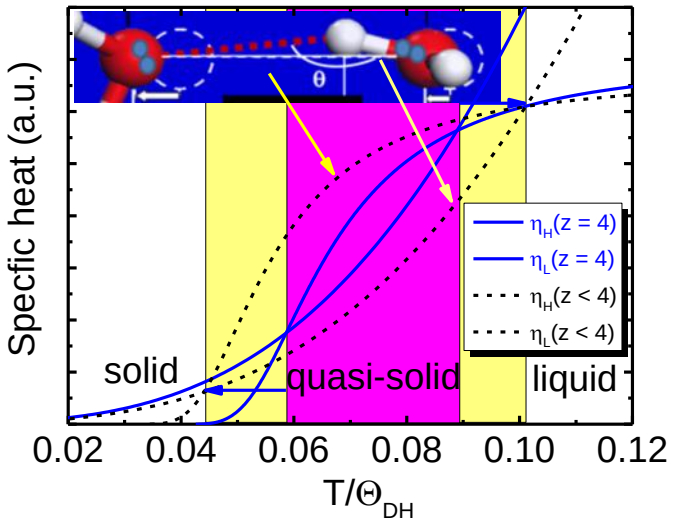

It has long been puzzling that water droplets undergo "supercooling" at freezing and "supercooling" at melting despite intensive investigation. With the involvement of undercoordinated skin molecules such as water droplets encapsulated in hydrophobic capillaries[1,2] and ultrathin water films deposited on graphite, silica, and certain metals [3-11] behave like ice at room temperature. The transition temperature for liquid formation (T_m) shifts from the bulk value of 273 K[12] up to 310 K for the skin[13] and 325 K for the monolayer film[14]; the homogeneous ice nucleation temperature (T_N) drops from the bulk value of 258 K[12] to 242 for 4.4 nm and 220 K for 3.4 nm[15], 205 K for 1.4 nm[16] and 172 K for 1.2 nm sized droplets [17]. Freezing transition for clusters containing 1-18 molecules cannot be observed at temperature down to120 K.[18]

The T_m elevation is more apparent at the curved skin because of its even lower coordinated molecules compared with those on a flat skin. For instances, a water droplet on a roughened Ag surface having a greater contact angle and higher curvature freezes 68.4 seconds later than the droplet on a smooth Ag surface at -4°C [19]. Transiting the initial contact angles of water droplet on quartz at 27.9°, on sapphire at 64.2°, and on graphite at 84.7° to zero requires heating to 185, 234, and 271°C, respectively[20]. Sum frequency generation spectroscopy revealed that the skin of two adjacent molecular layers are highly ordered at the hydrophobic contacts compared with those at the flat water-air interface[21]. An air gap of 0.5 ~ 1.0 nm thick exiting in the hydrophobic contacts[22] increases with the contact angle of the droplet or with the lowering of the effective coordination number (CN) of molecules at the skin.

It is yet unclear why the undercoordinated water molecules undergo both T_N depression and T_m elevation and why molecules are thermally more stable in the curved skins. Furthermore, the droplet size dependence of the T_N depression and T_m elevation is often referred to "supercooling" and "superheating" with unclear reasons [23]. In fact, supercooling, also known as undercooling [23], is the process of lowering the temperature of a liquid or a gas below its freezing point without it becoming a solid. Superheating is the opposite. Supercooled water occurs in the form of small droplets in clouds and plays a key role in the processing of solar and terrestrial radiative energy fluxes. Supercooled water is also important for life at subfreezing conditions for the commercial preservation of proteins and cells, and for the prevention of hydrate formation in nature gas pipelines. This communication aims to resolving this puzzle of droplet size induced T_N depression and T_m elevation based on the recent progress in understanding water and ice [12,13,24-30].

Generally, melting a specific atom inside a solid requires heat that is a fraction of its cohesive energy, $E_C = zE_z$, i.e., the sum of bond energy E_z over its coordination neighbors (z or CN). The T_m of a solid

changes with the solid size because of the skin atomic undercoordination induced bond order-length-strength (BOLS) correlation and the varied fraction of undercoordinated skin atoms[31]. Atomic undercoordination shortens and stiffens the bond between undercoordinated atoms, which differentiates the $E_C = zE_z$ at the skin from that of the bulk and hence governs the T_m of a nanosolid. The T_m usually drops with the inverse solid size because of the fraction change of undercoordinated atoms[32]. However, the presence of the critical temperatures at 273 K (T_m) and 258 K (T_N) for transiting the bulk liquid into the quasi-solid and then into ice[12] indicates that a quasi-solid (or quasi-liquid) phase exists in this temperature regime, which follows a different rule of thermodynamics.

Firstly, one has to consider the specific-heat per bond $\eta(T/\Theta_D)$ in Debye approximation when dealing with the thermodynamic behaviour of a substance from the atomistic point of view. The specific-heat is regarded as a macroscopic quantity integrated over all bonds of the specimen, which is also the amount of energy required to raise the temperature of the substance by 1 °C. The specific-heat per bond is obtained by dividing the bulk specific-heat by the total number of bonds involved [33]. For other usual materials, one bond represents all on average, and therefore, the thermal response of all the bonds are the same, without any discrimination in responding to thermal excitation [34].

However, for water ice, the representative hydrogen bond (O:H-O) is composed of two segments with strong disparity in the specific-heat of Debye approximation $\eta_x(T/\Theta_{Dx})$, as illustrated in Figure 1(O:H-O with ":" denoting the electron lone pair of oxygen; x = L and H denotes the O:H and the H-O segment, respectively). The O:H-O bond forms between O^{2-} ions (instead of between molecules) with asymmetric and short-range interactions, and importantly the Coulomb repulsion between electron pairs on oxygen ions. At the standard ambient condition (4 °C and atmospheric pressure, 0.1 MPA), the H-O bond is 1.0004 Å long with about 0.1 eV cohesive energy; the O:H nonbond is 1.6964 Å long and about 4.0 eV energy[12].

Parameters characterize the $\eta_x(T/\Theta_{Dx})$ include the Debye temperature Θ_{Dx} and its thermal integration. The Θ_{Dx}, which is lower than the T_{mx}, determines the speed of the $\eta_x(T/\Theta_{Dx})$ curve reaching saturation. The $\eta_x(T/\Theta_{Dx})$ curve of the segment with a relatively lower Θ_{Dx} value will rise to saturation quicker than the other segment does. The Θ_{Dx} is proportional to the characteristic frequency of vibration ω_x, following Einstein's relastion: $\hbar\omega_x = k\Theta_{Dx}$ with $\hbar$ and k being constant.

On the other hand, the integral of the $\eta_x(T/\Theta_{Dx})$ curve from 0 K to the T_{mx} is proportional to the cohesive energy E_x per segment [33]. The T_{mx} is the temperature at which the vibration amplitude of an atom/molecule expands abruptly to more than 3% of its diameter irrespective of the environment or the size of a molecular cluster [35,36].

Thus, with the known values of $\omega_L \sim 200$ cm^{-1} for O:H stretching and $\omega_H \sim 3200$ cm^{-1} for H-O stretching [12], $\Theta_{DL} = 198$ K < 273 K (T_m), $E_L = 0.095$ eV [37], and $E_H = 3.97$ eV [24], one can estimate $\Theta_{DH} \approx 16 \times \Theta_{DL} \approx 3200$ K and $T_{mH} >> \Theta_{DH}$ from the following,

$$\begin{cases} \Theta_{DL} / \Theta_{DH} \approx 198/\Theta_{DH} \approx \omega_L / \omega_H \approx 200/3200 \sim 1/16 \\ \left(\int_0^{T_{mH}} \eta_H dt \right) / \left(\int_0^{T_{mL}} \eta_L dt \right) \approx E_H / E_L \approx 4.0/0.1 \sim 40 \end{cases} \quad (1)$$

The η_L ends at $T_{mL} = 273$ K and the η_H ends at $T_{mH} \sim 3200$ K, which means that the area covered by the η_H curve is 40 times that covered by the η_L curve.

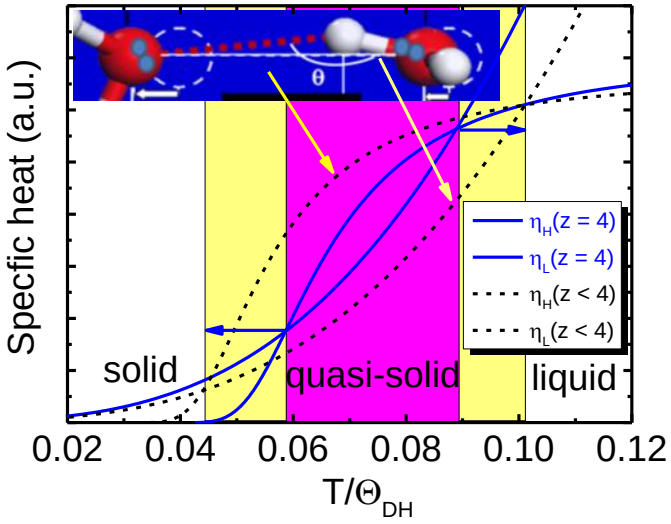

Figure 1 Illustration of the segmental specific-heat disparity of the O:H-O bond (inset; paring dots denote electron pairs on O^{2-} ions) and its evolution with the coordination number (z) of water molecules. Superposition of the specific-heat $\eta_x(T)$ curves for the O:H nonbond and the H-O bond defines two intersecting temperatures T_m and T_N that form the boundaries of the quasi-solid phase. Molecular undercoordination (z < 4) stretches $\eta_H(T/\Theta_{DH})$ by raising the $\Theta_{DH}(\omega_H)$ and depresses the $\eta_L(T/\Theta_{DL})$ by

lowering the $\Theta_{DL}(\omega_L)$, which disperses the intersecting temperatures in opposite directions. Therefore, a nanodroplet undergoes T_N depression and T_m elevation simultaneously and the extent of dispersion varies with the fraction of undercoordinated molecules of the droplet.

Secondly, a superposition of these two η_x curves makes the heat capacity of water ice to be different from those of other regular materials. Such a specific-heat superposition defines two intersecting temperatures that divide the full temperature range into water phases of liquid, quasi-solid/liquid, and solid with different η_L/η_H ratios. The inter-electron-pair repulsion and the external stimulus dislocate the O ions in the same direction but by different amounts. The weaker O:H always relaxes more than the H-O does. Therefore, in the liquid and in the solid phase ($\eta_L/\eta_H < 1$), the O:H nonbond contracts more than the H-O expands at cooling, resulting in the cooling densification of water and ice [15,16]; in the quasi-solid phase, the O:H and the H-O swap roles ($\eta_H/\eta_L < 1$), the H-O contracts less than the O:H expands at cooling, so the $\Delta d_{OO} > 0$ and water in quasi-solid phase become less dense as it cools, which is responsible for ice floating[12]. At the quasi-solid phase boundaries ($\eta_H/\eta_L = 1$), Δd_L and Δd_H transit in sign, which correspond to density extremes. Ideally, the T_m corresponds to the maximal density at 4 °C liquid and the T_N the minimal density of crystal [15,16,38]. Figure 2a and b verifies these expectations using Molecular Dynamics calculations. Refs [12,24] described details of the calculation procedures using Sun's algorithm COMPASS27 code[39].

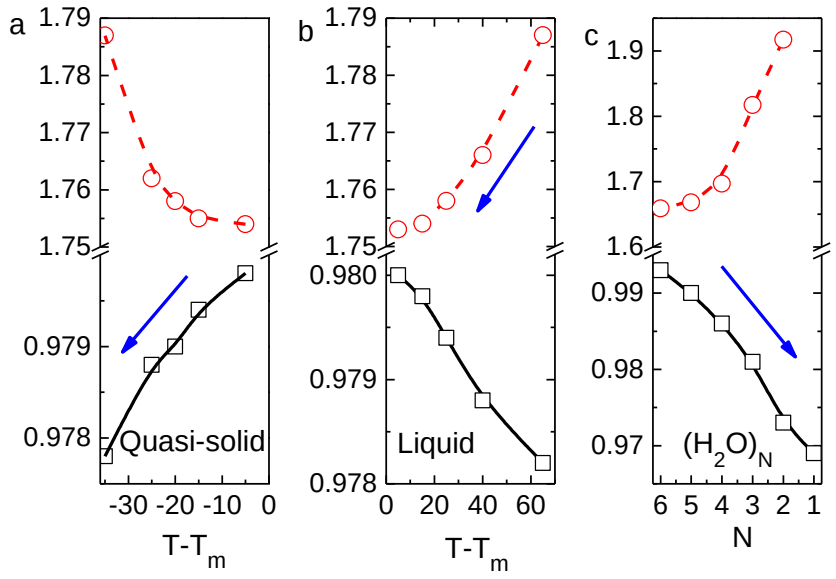

Figure 2. O:H-O bond segmental length response to: (b) cooling in the quasi–solid phase; (c) cooling in the liquid phase; and (d) $(H_2O)_N$ cluster size reduction (molecular undercoordination). Arrows indicate the master segments driving the relaxation dynamics.

One can imagine what will happen to the phase boundaries by raising the Θ_{DH} and meanwhile lowering the Θ_{DL}. The η_L will saturate quicker and the η_H slower than they were in the bulk case. This process will raise the T_m and lower the T_N, as illustrated in Figure 1a.

Strikingly, molecular undercoordination shortens the H-O bond and meanwhile lengthens the O:H nonbond, as shown in Figure 2c. Computations[13] also derived that the d_H contracts from the bulk value of about 1.00 to about 0.95 Å while the d_L elongates from about 1.68 to about 1.90 Å at the flat skin. This cooperative relaxation lengthens the O-O by 6.8% and reduces 18% skin mass density. Measurments also revealed that the distance between oxygen ions increases by 10% from the bulk value of 2.6950 Å to 2.9650 Å[40], which defines the segmental lengths of d_H = 0.8406 Å and d_L = 2.1126 Å[26], associated with a 0.75 g·cm^{-3} skin mass density[41]. The extrely low mass density, high eleasticty, high thermal stability, and strong polrization entitle the sperdolidity nature to be responsible for the sliperiness of ice and for the toughness and hyphodrobicity of water skin [13].

This O:H-O copperativ erelaxation due to molecular underoordination stiffens the ω_H phonon and softens the ω_L phonon[42], and shifts the O 1s binding energy positively as well. It has been confirmed that [43-47] the ω_H has a peak centered at 3200 cm^{-1} for bulk water, and at 3450 cm^{-1} for the skins of water ice; the ω_H for gaseous molecules is around 3650 cm^{-1}. The ω_H shifts from 3200 to 3650 cm^{-1} when the N of the $(H_2O)_N$ cluster drops from 6 to 1 [44,48,49]. Furthermore, molecular undercoordination shifts the O 1s energy level more deeply from the bulk value of 536.6 eV to 538.1 eV and 539.7 eV when bulk water is transformed into skin or into gaseous molecules[50-52].

Thirdly, as illustrated in Figure 3, the $(H_2O)_N$ size effect on the ω_x and on the η_{DH} curve for illustration. N-reduction-stiffened ω_H is consistent with spectroscopic measurements (scattered data). For instance, reduction of the $(H_2O)_N$ cluster from N = 6 to 1 stiffens the ω_H from 3200 to 3650 cm^{-1} and meanwhile softens the ω_L from 260 to 170 cm^{-1} as the bulk water turns into dimers[48]. Indeed, molecular undercoordination shortens and stiffens the H-O bond, and lengthens and softens the O:H nonbond consistently. Therefore, molecular undercoordination disperses indeed the quasi-solid phase boundaries through $\Theta_{Dx}(\omega_x)$ relaxation. According to the relationship in eq (1) (Θ_{DL}= 198 K, Θ_{DH} = 3200 K) and data in Figure 3a, the $\Theta_{Dx} \approx \omega_x$ in absolute values though the calculated ω_D is subject to modification with respect to measurements and ω_L is experimentally hardly avaiable[12]. We can estimate Θ_{DL} =198

(nulk)/260(calculated bulk)×195(calculated cluster) = 149 K and Θ_{DH} =3200/3200×3550 = 3550 K (for N = 2).

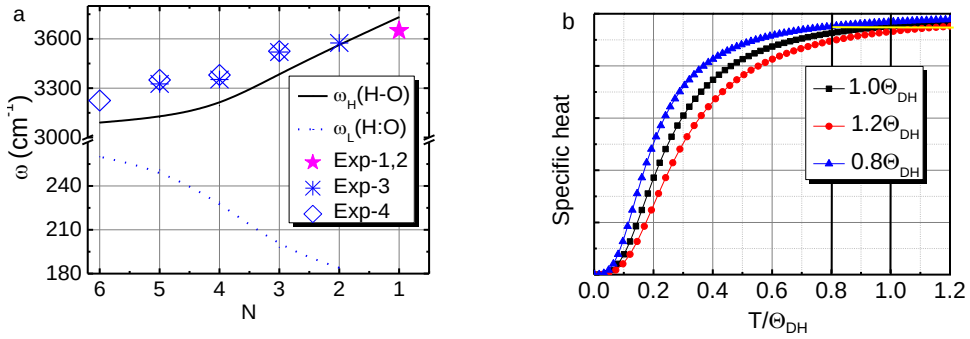

Figure 3. (a) Molecular undercoordination raised ω_H and depressed ω_L in $(H_2O)_N$ clusters in comparison with (scattered data) measurements shown as Exp-1 [47], Exp-2 [48], Exp-3 [44], and Exp-4 [49]. (b) Illustration of the η_H modulation by $\Theta_{DH}(\omega_H)$ relaxation.

Finally, understandings may extend to the thermodynamic behavior of water droplets and gas bubbles at the nanometer scales. These systems of undercoordinated molecular dominance have far-reaching physical, chemical, and biological effects [53] because molecular undercoordination induced unusual bond-electron-phonon behavior, as afore discussed. They are hardly destroyed and thermally much more stable than bubbles at the millimeter scale [54]. Water nanodroplets and nanobubbles do follow the trend of T_m elevation and T_N depression because of the dominant fraction of undercoordinated skin molecules. Droplet size reduction raises the $\Theta_{DH}(\omega_H)$ and stretches the $\eta_H(T)$ curve and meanwhile, lowers the Θ_{DL}-(ω_L) and compresses the $\eta_L(T)$ curve, which disperses the extreme-density temperatures. A bubble is just the inversion of a droplet; a hollow sphere like a soap bubble contains two skins – the inner and the outer. Both skins are in the supersolid phase and the volume fraction of such supersolid phase over the entire liquid-shell volume is much greater than simply a droplet. Therefore, bubbles demonstrate more significantly the supersolidity nature – elastic, hydrophobic, and thermally stable, which makes bubbles mechanically stronger and thermally more stable[13].

In summary, water molecular undercoordination shortens the H-O bond and stiffens its phonon spontaneously. The O:H nonbond responds oppositely to undercoordination in length and phonon frequency. Such an O:H-O bond cooperative relaxation raises the Θ_{DH} and lowers the Θ_{DL} simultaneously, dispersing the quasi-soli phase boundaries. Therefore, H-O bond contraction elevates the melting point

and O:H nonbond elongation depresses the freezing temperature of water droplets and bubbles of which the undercoordinated molecules become dominant.

Acknowledgement

Financial support from National Natural Science Foundation (No. 21273191) of China is acknowledged.

References

(1) Lakhanpal, M. L.; Puri, B. R. Boiling Point of Capilary-Condensed Water. *Nature* **1953**, *172*, 917-917.

(2) Li, L.; Kazoe, Y.; Mawatari, K.; Sugii, Y.; Kitamori, T. Viscosity and Wetting Property of Water Confined in Extended Nanospace Simultaneously Measured from Highly-Pressurized Meniscus Motion. *J. Phys. Chem. Lett.* **2012**, 2447-2452.

(3) Xu, K.; Cao, P. G.; Heath, J. R. Graphene Visualizes the First Water Adlayers on Mica at Ambient Conditions. *Science* **2010**, *329*, 1188-1191.

(4) Xu, D.; Liechti, K. M.; Ravi-Chandar, K. Mechanical Probing of Icelike Water Monolayers. *Langmuir* **2009**, *25*, 12870-12873.

(5) Miranda, P. B.; Xu, L.; Shen, Y. R.; Salmeron, M. Icelike Water Monolayer Adsorbed on Mica at Room Temperature. *Phys. Rev. Lett.* **1998**, *81*, 5876-5879.

(6) McBride, F.; Darling, G. R.; Pussi, K.; Hodgson, A. Tailoring the Structure of Water at a Metal Surface: A Structural Analysis of the Water Bilayer Formed on an Alloy Template. *Phys. Rev. Lett.* **2011**, *106*, 226101.

(7) Hodgson, A.; Haq, S. Water Adsorption and the Wetting of Metal Surfaces. *Surf. Sci. Rep.* **2009**, *64*, 381-451.

(8) Meng, S.; Wang, E. G.; Gao, S. W. Water Adsorption on Metal Surfaces: A General Picture from Density Functional Theory Studies. *Phys. Rev. B* **2004**, *69*, 195404.

(9) Wang, C.; Lu, H.; Wang, Z.; Xiu, P.; Zhou, B.; Zuo, G.; Wan, R.; Hu, J.; Fang, H. Stable Liquid Water Droplet on a Water Monolayer Formed at Room Temperature on Ionic Model Substrates. *Phys. Rev. Lett.* **2009**, *103*, 137801-137804.

(10) Michaelides, A.; Morgenstern, K. Ice Nanoclusters at Hydrophobic Metal Surfaces. *Nat. Mater.* **2007**, *6*, 597-601.

(11) Johnston, J. C.; Kastelowitz, N.; Molinero, V. Liquid to Quasicrystal Transition in Bilayer Water. *J Chem Phys* **2010**, *133*.

(12) Sun, C. Q.; Zhang, X.; Fu, X.; Zheng, W.; Kuo, J.-l.; Zhou, Y.; Shen, Z.; Zhou, J. Density and Phonon-Stiffness Anomalies of Water and Ice in the Full Temperature Range. *J Phys Chem Lett* **2013**, *4*, 3238-3244.

(13) Zhang, X.; Huang, Y.; Ma, Z.; Zhou, Y.; Zheng, W.; Zhou, J.; Sun, C. Q. A Common Supersolid Skin Covering Both Water and Ice. *PCCP* **2014**, *16*, 22987-22994.

(14) Qiu, H.; Guo, W. Electromelting of Confined Monolayer Ice. *Phys. Rev. Lett.* **2013**, *110*, 195701.

(15) Erko, M.; Wallacher, D.; Hoell, A.; Hauss, T.; Zizak, I.; Paris, O. Density Minimum of Confined Water at Low Temperatures: A Combined Study by Small-Angle Scattering of X-Rays and Neutrons. *PCCP* **2012**, *14*, 3852-3858.

(16) Mallamace, F.; Branca, C.; Broccio, M.; Corsaro, C.; Mou, C. Y.; Chen, S. H. The Anomalous Behavior of the Density of Water in the Range 30 K < T < 373 K. *PNAS* **2007**, *104*, 18387-18391.

(17) Alabarse, F. G.; Haines, J.; Cambon, O.; Levelut, C.; Bourgogne, D.; Haidoux, A.; Granier, D.; Coasne, B. Freezing of Water Confined at the Nanoscale. *Phys. Rev. Lett.* **2012**, *109*, 035701.

(18) Moro, R.; Rabinovitch, R.; Xia, C.; Kresin, V. V. Electric Dipole Moments of Water Clusters from a Beam Deflection Measurement. *Phys. Rev. Lett.* **2006**, *97*, 123401.

(19) Singh, D. P.; Singh, J. P. Delayed Freezing of Water Droplet on Silver Nanocolumnar Thin Film. *Appl. Phys. Lett.* **2013**, *102*, 243112.

(20) Friedman, S. R.; Khalil, M.; Taborek, P. Wetting Transition in Water. *Phys. Rev. Lett.* **2013**, *111*.

(21) Strazdaite, S.; Versluis, J.; Backus, E. H.; Bakker, H. J. Enhanced Ordering of Water at Hydrophobic Surfaces. *J Chem Phys* **2014**, *140*, 054711.

(22) Uysal, A.; Chu, M.; Stripe, B.; Timalsina, A.; Chattopadhyay, S.; Schlepütz, C. M.; Marks, T. J.; Dutta, P. What X Rays Can Tell Us About the Interfacial Profile of Water near Hydrophobic Surfaces. *Phys. Rev. B* **2013**, *88*, 035431.

(23) Debenedetti, P. G.; Stanley, H. E. Supercooled and Glassy Water. *Phys. Today* **2003**, *56*, 40-46.

(24) Sun, C. Q.; Zhang, X.; Zhou, J.; Huang, Y.; Zhou, Y.; Zheng, W. Density, Elasticity, and Stability Anomalies of Water Molecules with Fewer Than Four Neighbors. *J. Phys. Chem. Lett.* **2013**, *4*, 2565-2570.

(25) Sun, C. Q.; Zhang, X.; Zheng, W. T. Hidden Force Opposing Ice Compression. *Chem Sci* **2012**, *3*, 1455-1460.

(26) Huang, Y.; Zhang, X.; Ma, Z.; Zhou, Y.; Zhou, J.; Zheng, W.; Sun, C. Q. Size, Separation, Structure Order, and Mass Density of Molecules Packing in Water and Ice. *Scientific Reports* **2013**, *3*, 3005.

(27) Huang, Y.; Zhang, X.; Ma, Z.; Zhou, Y.; Zhou, G.; Sun, C. Q. Hydrogen-Bond Asymmetric Local Potentials in Compressed Ice. *J. Phys. Chem. B* **2013**, *117*, 13639-13645.

(28) Zhang, X.; Yan, T.; Huang, Y.; Ma, Z.; Liu, X.; Zou, B.; Sun, C. Q. Mediating Relaxation and Polarization of Hydrogen-Bonds in Water by Nacl Salting and Heating. *PCCP* **2014**, *16*, 24666-24671.

(29) Zhang, X.; Huang, Y.; Ma, Z.; Zhou, Y.; Zhou, J.; Zheng, W.; Jiang, Q.; Sun, C. Q. Hydrogen-Bond Memory and Water-Skin Supersolidity Resolving the Mpemba Paradox. *PCCP* **2014**, *16*, 22995-23002.

(30) Huang, Y.; Zhang, X.; Ma, Z.; Zhou, Y.; Zheng, W.; Zhou, J.; Sun, C. Q. Hydrogen-Bond Relaxation Dynamics: Resolving Mysteries of Water Ice. *Coord. Chem. Rev.* **2015**, *285*, 109-165.

(31) Sun, C. Q. *Relaxation of the Chemical Bond*; Springer: Heidelberg, 2014 Vol. 108.

(32) Sun, C. Q. Size Dependence of Nanostructures: Impact of Bond Order Deficiency. *Prog. Solid State Chem.* **2007**, *35*, 1-159.

(33) Sun, C. Q. Thermo-Mechanical Behavior of Low-Dimensional Systems: The Local Bond Average Approach. *Prog. Mater Sci.* **2009**, *54*, 179-307.

(34) Gu, M. X.; Zhou, Y. C.; Sun, C. Q. Local Bond Average for the Thermally Induced Lattice Expansion. *J. Phys. Chem. B* **2008**, *112*, 7992-7995.

(35) Omar, M. A. *Elementary Solid State Physics: Principles and Applications*; Addison-Wesley: New York, 1993.

(36) Lindemann, F. A. The Calculation of Molecular Natural Frequencies. *Phys. Z.* **1910**, *11*, 609-612.

(37) Zhao, M.; Zheng, W. T.; Li, J. C.; Wen, Z.; Gu, M. X.; Sun, C. Q. Atomistic Origin, Temperature Dependence, and Responsibilities of Surface Energetics: An Extended Broken-Bond Rule. *Phys. Rev. B* **2007**, *75*, 085427.

(38) Moore, E. B.; Molinero, V. Structural Transformation in Supercooled Water Controls the Crystallization Rate of Ice. *Nature* **2011**, *479*, 506-508.

(39) Sun, H. Compass: An Ab Initio Force-Field Optimized for Condensed-Phase Applicationsoverview with Details on Alkane and Benzene Compounds. *J. Phys. Chem. B* **1998**, *102*, 7338-7364.

(40) Wilson, K. R.; Schaller, R. D.; Co, D. T.; Saykally, R. J.; Rude, B. S.; Catalano, T.; Bozek, J. D. Surface Relaxation in Liquid Water and Methanol Studied by X-Ray Absorption Spectroscopy. *J Chem Phys* **2002**, *117*, 7738-7744.

(41) Zhang, X.; HUang, Y.; Ma, Z.; Zhou, J.; Zhou, Y.; Zheng, W.; Sun, C. Q. A Common Superslid Skin Covering Both Water and Ice. *PCCP* **2014**, DOI: 10.1039/C1034CP02516D.

(42) Sun, C. Q.; Zhang, X.; Zhou, J.; Huang, Y.; Zhou, Y.; Zheng, W. Density, Elasticity, and Stability Anomalies of Water Molecules with Fewer Than Four Neighbors. *J Phys Chem Lett* **2013**, *4*, 2565-2570.

(43) Kahan, T. F.; Reid, J. P.; Donaldson, D. J. Spectroscopic Probes of the Quasi-Liquid Layer on Ice. *J Phys Chem A* **2007**, *111*, 11006-11012.

(44) Ceponkus, J.; Uvdal, P.; Nelander, B. Water Tetramer, Pentamer, and Hexamer in Inert Matrices. *J Phys Chem A* **2012**, *116*, 4842-4850.

(45) Shen, Y. R.; Ostroverkhov, V. Sum-Frequency Vibrational Spectroscopy on Water Interfaces: Polar Orientation of Water Molecules at Interfaces. *Chem. Rev.* **2006**, *106*, 1140-1154.

(46) Buch, V.; Bauerecker, S.; Devlin, J. P.; Buck, U.; Kazimirski, J. K. Solid Water Clusters in the Size Range of Tens-Thousands of H2o: A Combined Computational/Spectroscopic Outlook. *Int. Rev. Phys. Chem.* **2004**, *23*, 375-433.

(47) Cross, P. C.; Burnham, J.; Leighton, P. A. The Raman Spectrum and the Structure of Water. *J Am Chem Soc* **1937**, *59*, 1134-1147.

(48) Sun, Q. The Raman Oh Stretching Bands of Liquid Water. *Vib. Spectrosc* **2009**, *51*, 213-217.

(49) Hirabayashi, S.; Yamada, K. M. T. Infrared Spectra and Structure of Water Clusters Trapped in Argon and Krypton Matrices. *J. Mol. Struct.* **2006**, *795*, 78-83.

(50) Abu-Samha, M.; Borve, K. J.; Winkler, M.; Harnes, J.; Saethre, L. J.; Lindblad, A.; Bergersen, H.; Ohrwall, G.; Bjorneholm, O.; Svensson, S. The Local Structure of Small Water Clusters: Imprints on the Core-Level Photoelectron Spectrum. *Journal of Physics B-Atomic Molecular and Optical Physics* **2009**, *42*, 055201.

(51) Nishizawa, K.; Kurahashi, N.; Sekiguchi, K.; Mizuno, T.; Ogi, Y.; Horio, T.; Oura, M.; Kosugi, N.; Suzuki, T. High-Resolution Soft X-Ray Photoelectron Spectroscopy of Liquid Water. *PCCP* **2011**, *13*, 413-417.

(52) Winter, B.; Aziz, E. F.; Hergenhahn, U.; Faubel, M.; Hertel, I. V. Hydrogen Bonds in Liquid Water Studied by Photoelectron Spectroscopy. *J Chem Phys* **2007**, *126*, 124504.

(53) Chaplin, M. Water Structure and Science: Http://Www.Lsbu.Ac.Uk/Water/.

(54) Tyrrell, J. W. G.; Attard, P. Images of Nanobubbles on Hydrophobic Surfaces and Their Interactions. *Phys. Rev. Lett.* **2001**, *87*, 176104.